doi:10.2533/chimia.2022.846 Chimia 76 (2022) 846–851

(Anti)viral Material Design Guided by Scattering Methods

Samuel Watts[#], Bettina Tran[#], and Stefan Salentinig*

Abstract: Viruses are nature's nanoparticles that are highly symmetric and monodisperse in size and shape with well-defined surface chemistry. They have evolved for optimal cell interactions, genetic information delivery, and replication by the host cell over millions of years. These features render them highly efficient pathogens that place a severe burden on the health of our society. At the same time, they are fascinating objects for colloidal studies and as building blocks for advanced bio-inspired materials. Their characterisation requires sophisticated experimental techniques such as X-ray, neutron, and light scattering that allow probing the structures and interactions on a nanometre to micrometre length scale in solution. This contribution summarises the recent progress in virus self-assembly and virus-based biopolymer composites for advanced material design. It discusses the advances and highlights challenges in characterising structures and dynamics in these materials, focusing on scattering techniques. It further demonstrates selected applications in the field of food and water purification.

Keywords: Antiviral materials · cryo-TEM · DLS · Scattering methods · SANS · SAXS · Virus-based material · Virus self-assembly

Samuel Watts is a post-doctoral researcher in the Biocolloids lab working on antibacterial surfaces at the University of Fribourg. He previously earned a PhD from ETH for his work done at Empa. He focused on scattering methods to investigate virus colloidal structures to design the virus removal process from drinking water and antiviral materials. He has been awarded an SNSF mobility fellowship to pursue research in the creation of functional bacteriophage material in the Bioengineered and Applied Nanomaterials Laboratory at Nanyang Technological University in Singapore.

Bettina Tran is a PhD student in the Biocolloids lab at the University of Fribourg. Her research focuses on the precision synthesis of antimicrobial polymers and their interactions with bacteria and viruses for novel antimicrobial biomaterials. She obtained her Bachelor's and Master's degrees in material science from ETH Zürich, where she researched non-flammable foam for insulation from waste material and environmentally-friendly aqueous processing of recombinant spider silk.

Stefan Salentinig is a professor in physical chemistry at the University of Fribourg, where he established the Biocolloids lab, researching bio-inspired materials for food and health applications. He holds a PhD in physical chemistry focusing on food colloids and scattering methods from the University of Graz, Austria, in 2010. He then moved to Australia to take on a scientist position on separation technology at the CSIRO. He became a lecturer at Monash University in Melbourne, working on nanoscale drug delivery systems. In 2015, he joined the Swiss Federal Labs (Empa) as a group leader on functional materials before starting his current role in 2019.

1. Introduction: Virus and Bacteriophages

Viruses are nature's nanoparticles that deliver genetic information to targeted cells for replication. The basic structure of most viruses is a highly symmetric protein cage formed through the self-assembly of multiple copies of peptide subunits surrounding the genetic material in the core. This cage is remarkably uniform in size and shape, primarily spherical or rod-like (Fig. 1).[1] It possesses well-defined surface chemistry to trigger specific interactions with the host cells. These features make viruses fascinating objects for fundamental colloid and interface science studies and promising subunits for advanced functional biomaterials for applications, amongst others, in the food and health science fields.[1]

Non-enveloped viruses consist only of the protein nanocage loaded with genetic material. Amongst these species are most water-borne gastrointestinal viral pathogens, including rotavirus and norovirus.[6] This class also contains non-pathogenic viruses, including most bacteriophages (bacteria viruses) and plant viruses that are interesting for their antibacterial and scaffold properties.[1,7]

More complex enveloped viruses have an additional lipid envelope surrounding the protein cage. The lipid envelope comes from the host cell's plasma membrane. It embeds the host–cell recognition proteins (Fig. 1). Some of the most problematic pathogenic viruses, including influenza, SARS-CoV-2, Ebola, and HIV, belong to this class.[8] Enveloped non-pathogenic phages and plant viruses are rare compared to their non-enveloped counterparts. However, the enveloped bacteriophage Phi6 is frequently used as enveloped virus surrogate for fundamental studies.[5]

Non-covalent interactions among the virus protein and the lipid sub-units, as well as between the virus and other materials in the surrounding, including other viruses, cells, material surfaces, and biopolymers, dictate the fate of the virus. Hence, understanding these interactions is crucial in guiding the design of virus-based biomaterials and for virus remediation and antiviral strategies.

*Correspondence: Prof. Dr. S. Salentinig, E-mail: stefan.salentinig@unifr.ch
Dept. Chemistry, University of Fribourg, Chemin Du Musée 9, CH-1700 Fribourg
[#]Contributed equally

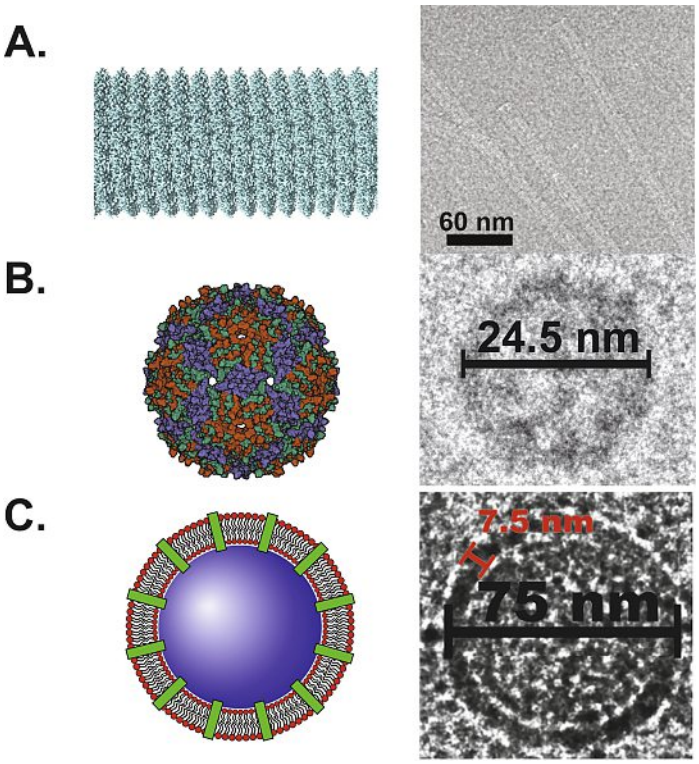

Fig. 1. A) Protein reconstruction and cryo-TEM image of the rod-like Tobacco mosaic virus. Adapted from ref. [2]. Copyright 2011 National Academy of Sciences. B) Protein reconstruction of the spherical bacteria virus MS2. Adapted from PDB databank,[3] and cryo-TEM adapted with permission from ref. [4]. Copyright 2020 American Chemical Society. C) Schematic representation of an enveloped virus with a corresponding cryo-TEM image of the enveloped bacteria virus Phi6 adapted with permission from ref. [5]. Copyright 2021 American Chemical Society.

The in-depth study of these interactions requires advanced characterisation techniques that allow to probe the length scales from the nanometre to the micrometre region in a non-invasive manner. Scattering techniques are the methods of choice for this purpose as they provide statistical information on structure within this size range, provided the correct wavelength is chosen.[9]

This contribution discusses the application of scattering techniques to investigate the structure and interaction of materials and their implications for the design of novel nanostructured biomaterials.

2. Scattering Methods for Virus Characterisation

Static and dynamic scattering methods are non-invasive techniques that are well-suited to study virus-based colloids. They provide statistical information on the size, shape, morphology, and stability of nanoparticles such as viruses.[9]

The minimum and maximum structural dimensions probed with scattering depend on the wavelength of the radiation and the angular range for intensity detection (scattering angle). In general, larger structures scatter to smaller angles. Thus, small angle X-ray and neutron scattering (SAXS and SANS), operating at a small wavelength, cover the size range between 1–100 nm, corresponding to scattering angles down to 0.1°. The instrumentation and methodology have been reviewed recently.[10] In combination with a high-intensity X-ray source and microfluidics or stopped flow approaches, SAXS can be used for *in situ* studies of colloidal transformations, as demonstrated previously.[11] Ultra-small angle scattering (USAXS / USANS), operating at even lower angles, provides information up to the micrometre range. Static light scattering, operating at a much larger wavelength, covers the size range from hundreds of nanometres to micrometres.

Small angle scattering techniques provide structural information in the inverse (Fourier) space. The signal combines intra-particle correlations (form factor) and inter-particle correlations (structure factor). The form factor scattering contains information on the particles' size, shape, and morphology; and the structure factor on the organisation of the particles in solution from which their interaction potential can be derived. The separation of the experimental scattering intensity into the two components is mathematically an ill-defined problem. Several solutions have been suggested to separate the two factors. The most straightforward approach is practical with dilution experiments to low-enough concentrations. The structure factor scattering is concentration dependent and reaches unity at low-enough particle concentrations, providing the form factor scattering only. Other mathematical methods exist that fit the form and structure factor parameters simultaneously.

Important sample parameters, such as the radius of gyration (R_g), the surface-to-volume ratio, or the folding of proteins, can be extracted directly from the form factor scattering. More sophisticated mathematical data-modelling approaches are necessary to extract information on size, shape, morphology, and interaction potential. Model-free and model-dependent methods exist for this purpose.

The model-free indirect Fourier transformation method (IFT) is a powerful tool for evaluating form factor scattering.[12] The method was extended to approximate simultaneously the structure factor based on specific structure factor models such as hard sphere (excluded volume interactions) and charged sphere. This was called the generalised IFT (GIFT) method.[13] This method provides the pair distance distribution function, $p(r)$, from the $I(q)$ in a model-free approach.[13] The $p(r)$ enables the determination of the overall shape and size of the scattering objects in real space.[12,14]

The deconvolution of the $p(r)$ gives the radial contrast profile in electron density relative to the solvent by assuming spherical, cylindrical, or a bilayer symmetry of the scattering particles.[14,15] This profile in electron density contains information about the internal structure of the scattering particles. The procedure is summarised for the bacteria virus MS2 in Fig. 2.[4] The symmetric $p(r)$ function indicates that the virus particles are approximately spherical with a diameter, D, of 27 nm, from $p(r) = 0$. By a convolution square-root operation, the deconvolution of the $p(r)$ generates the averaged radial excess electron density profile of the virus particles relative to the surrounding buffer. The point of inflection in this profile, between the core and shell regions, provides an estimate for the radius of the virus core and the protein shell. The core radius is around 8 nm, and the overall particle radius is about 13.5 nm, in reasonable agreement with the radius from the $p(r)$ analysis at $D/2$ (Fig. 2). This evaluation was further backed-up with the model-dependent fitting of the form factor scattering, where the theoretical scattering curve for the virus' spherical core-shell geometry is approximated. The parameters such as size, differences in the excess electron densities, and morphology are optimised to obtain the best possible fit of the model to the experimental data.[4,16]

The model-independent scattering data evaluation was recently used to research the ethanol inactivation of enveloped viruses.[5] The SAXS patterns of the lipid-enveloped bacteria virus are characteristic of bilayer structures.[17] In this case, the thickness pair distance distribution function, $p_t(r)$, of the lipid bilayer surrounding the protein cage could be calculated from the data.[18] It indicated higher electron density in the charged head groups, with associated counter-ions, and lower electron density in the tails of the lipids relative to the electron density of the surrounding buffer.[19] However, deconvolution of the $p_t(r)$ into the corresponding excess electron density function was not possible, most probably due to the scattering contribution of the nucleocapsid on one bilayer side and buffer on the other leading

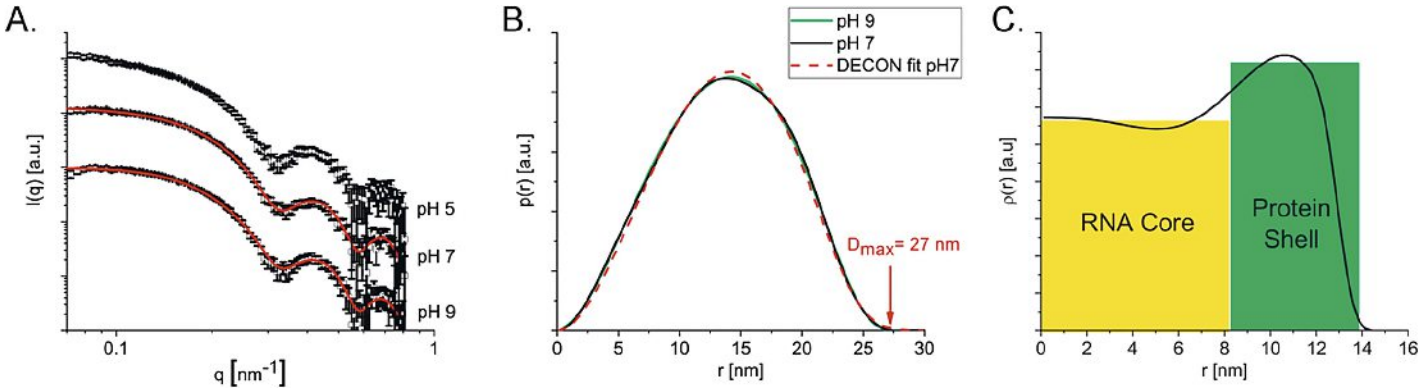

Fig. 2. (A) Experimental SAXS data (open squares) and corresponding fits (red lines) calculated using the generalised indirect Fourier transformation method for the bacteria virus MS2. (B) The corresponding pair distance distribution function of the virus at pH 7 and 9 from part A; and fit calculated from deconvolution using a convolution square root operation (red dashed line). (C) Radial excess electron density of the virus at pH 7, calculated from part B by deconvolution. Reprinted with permission from ref. [4]. Copyright 2020 American Chemical Society.

to deviations from the bilayer symmetry assumptions. This would require using SANS with so-called contrast matching techniques, which is part of an ongoing study in our team.

SANS probes a similar size range to SAXS. However, electrons scatter X-rays, whereas neutrons are scattered by the atomic nucleus. Hence, the scattering contrast in SAXS arises from differences in electron densities; and SANS from differences in the scattering length densities of the nuclei. A key feature of SANS is that the scattering contrast can be modified by replacing hydrogen with its heavier isotope, deuterium, as they have very different scattering length densities. Selective deuteration is useful, for instance, to change the scattering contrast of a specific part or molecule to map its location within a structure. We used a combination of SAXS and SANS, with contrast matching techniques and selective deuteration for mapping individual molecules in mixed micelles.[20] In solvent contrast matching measurements, the contrast between specific molecules can be enhanced or eliminated by mixing H_2O and D_2O in defined ratios. Hence, a feature in the particle with a similar scattering length density to that of the D_2O/H_2O buffer will yield negligible scattering intensity. A second approach is the selective deuteration of non-solvent molecules in the scattering particles.[20a,b] This selective deuteration can be applied to map the structure and morphology of the individual components in the nanocage, including the distribution of loaded guest molecules.

Operating at larger wavelengths, static light scattering resolves particle shape and interactions in the micrometre range. The contrast is given by the difference in polarisability between the scattering particles and the surrounding medium, which is linked to the refractive index difference. Dynamic light scattering (DLS) measures the collective diffusion of particles in a solution that can be converted to the hydrodynamic radius. It also provides information on the particle's interactions as they influence its diffusion.[21] The simultaneous measurement of DLS at multiple scattering angles (multi-angle DLS) allows the accurate analysis of multimodal systems and is especially valuable for studying particle aggregation processes.[22] This is based on the fact that each scattering angle gives a different weight to a specific particle size (based on the form factor scattering of the particle). Depolarized DLS provides access to other parameters, such as the translational and rotational contributions to diffusion in optically anisotropic particles such as elongated viruses.[23] For non-ergodic systems (gels), brute force or multi-speckle detection has been used to study the dynamics in the system.[24]

As a result of the indirect nature of scattering techniques, the results are highly dependent on the quality of the data analysis. The usage of relevant models and a systematic analysis yields otherwise inaccessible information. However, one has to be careful to avoid incorrect data handling and over-interpretation of the data. *A priori* knowledge from other methods, such as zeta-potential measurements and electron microscopy techniques, provides valuable information to limit variables during scattering data modelling. Together with biological evaluation studies, they allow for an advanced understanding of viral particle interactions and morphology to design advanced material, as highlighted in the following chapters.

3. Virus Colloidal Structure and Interaction in an Aqueous Environment

3.1 *Self-assembly of Non-enveloped Viruses in Solution, the Effect of pH and Ionic Strength*

The protein nanocage's net surface charge is defined by its amino acid composition and pH value.[25] Most viruses are negatively charged at pH values above 5, relevant for biological environments (blood) and drinking water.[26] These viruses are colloidally stabilised through electrostatic repulsions under these conditions.

The viruses' interaction potential can be modified with environmental parameters such as pH, ionic strength, and the type of ions in the solution. Multivalent ions are more efficient in reducing the Debye length than monovalent ones. They can also specifically interact with virus surface groups, such as amine, carboxyl, or thiol groups, leading to the bridging between particles.[27] For example, efficient coagulation of viruses with iron and aluminium salts in wastewater treatment has been reported.[28]

The pH value of the solution triggers the protonation (at low pH values) or deprotonation (at high pH values) of amine and carboxyl groups. Close to the viruses' isoelectric point, charge repulsion will diminish and result in aggregation.[29] This effect is shown for the non-enveloped bacteriophage MS2, whereby SAXS, DLS, cryo-TEM, and zeta-potential analysis confirmed the significant influence of the pH on the interparticle interaction.[4] The pH-triggered aggregation of the virus close to its isoelectric point was shown to be reversible upon pH circulation. Further, it could be demonstrated that the pH-triggered aggregation and dis-aggregation process had no significant influence on the structure of the virus cage. This pH-triggered reversible aggregation can be used to remove nanoscale viruses during conventional drinking water filtration processes. The non-enveloped viruses with diameters around 30 nm cannot be removed efficiently from water with traditional size-exclusion filtration processes. These filters only target micron-sized objects such as bacteria. However, pH-triggered virus aggregation at pH <5 leads to the formation of micron-sized aggregates that can then easily be removed with such conventional filters. Once the filter needs regeneration, a simple pH increase can induce the de-aggregation of the virus aggregates inside the filter and their removal by flushing.[30]

The interactions described above may also help ingested viruses transit through the digestive system: The viruses may aggregate in the stomach's acidic pH around 1 to 4, protecting the viruses inside the aggregate from protein digestion. The alkaline conditions in the small intestine (pH 6–8) can lead to the dispersion of the aggregate, with most of the virus particles intact and infective.

3.2 *Virus–Polymer Composites*

Specific interactions among molecules and viruses can be used to trigger the formation of virus composite materials. Molecules that specifically adsorb onto the virus surface modify the virus interactions and colloidal stability in solution. Attractive or repulsive interactions occur depending on the type of molecule and its concentration on the surface.[27,31]

The flocculation of viruses is heavily researched for separation processes, including water purification, for which virus removal is mainly studied with biological assays.[32] Chitosan-based polycationic polymers were reported as a coagulant.[28] Composition-dependent aggregation of polycationic polymers and viral particles leading to the formation of colloidal crystals for advanced biomaterial design is currently a research topic in our group.

The interaction of cationic nanocellulose (CNFC) and non-enveloped viruses was studied using SAXS, cryo-TEM, and zeta-potential measurements (Fig. 3).[30] The linear combinations of the SAXS curves of the two individual components were used to produce the best possible fit of the composite material's experimental SAXS curve. Without interactions, a good fit (low residuals) is expected as there are no additional contributions to either component's scattering or structural modification. In contrast, virus particles adsorbing to the nanocellulose would lead to low fit quality (high residuals), owing to the modified contributions of the form factors, structure factors, and scattering cross-term between CNFC surface and virus surface. This method demonstrated the pH-dependant behaviour of the virus and nanocellulose mixture. At pH 3, the virus and nanocellulose are positively charged, showing only little interaction. However, at pH >5, strong interactions were found among the oppositely charged compounds. The resulting structure can be observed in cryo-TEM (Fig. 3).

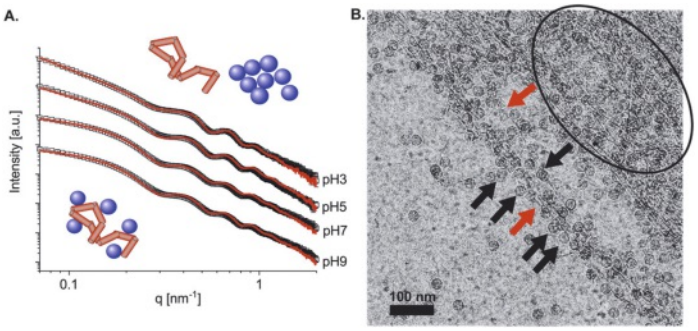

Fig. 3. Colloidal interactions between the non-enveloped bacteria virus Qbeta and cationic nanocellulose (CNFC). (A) Experimental SAXS data (open squares) for the 1:1 weight ratio of Qbeta and CNFC at pH values of 3, 5, 7, and 9. The corresponding fits (red curves) calculated with a linear combination of the experimental scattering curves from the pure species at the corresponding pH value are also shown. (B) cryo-TEM image of the mixture of Qbeta and CNFC at pH 7. Examples of CNFC are highlighted with red arrows, and Qbeta particles adsorbed on the CNFC with black arrows. A large aggregate of CNFC and Qbeta is highlighted with a black ellipse. Adapted from ref. [30] used under Creative Commons CC-BY license.

This structural knowledge allowed the design of a cellulose-based water filter with pH-dependent removal of viruses from water. The filter removes viruses at the pH of natural water and can be regenerated at acidic pH.[30]

Tailoring interactions between viruses allowed the design of highly structured materials with the potential for application, for instance, as nano templates.[33,34] In nature, the anionic biopolymers were found to induce the dense packing of the filamentous symbiotic Pf4 bacteria virus around *pseudomonas aeruginosa* bacteria, leading to increased resistance against tobramycin antibiotics.[35] The aggregates' liquid crystalline morphology was investigated by cryo-TEM.[35] Among the synthetic materials, the combination of nanometre-sized cationic polyamidoamine dendrimer with the quasi-spherical P22 bacteria virus of 56 nm and surface-modified variants led to the formation of superlattices with a dominant face-centred cubic structure and a minor hexagonal close-packed phase (Fig. 4).[31,33] SAXS was used to characterise the arrangement in the P22-dendrimer aggregates. It demonstrated the self-assembly across multiple length scales from the capsid protein to the particle superlattice. The particle's self-assembly into ordered structures could be modified by varying the ionic strength and the surface charge of the P22 virus, with the nearest neighbour distance of 62 nm. Depending on the P22 variant, those superlattices can have a domain size of over 400 nm and a lattice parameter of around 87 nm. These superlattices were applied to provide spatial separation for enzymes encapsulated into the protein cages and resulted in a more efficient isobutanol synthesis.[31,33]

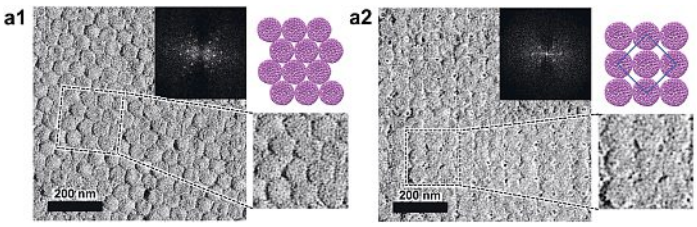

Fig. 4. TEM image of superlattices formed through virus/dendrimer interactions in solution. The fast Fourier transform of selected structured regions is presented as an inset and graphical view of the structures. A hexagonal closed-packed structure is shown in (a1), while an area with a face-centred cubic structure is presented in (a2). Adapted with permission from ref. [33]. Copyright 2017 American Chemical Society.

Highly ordered protein-cage aggregates were also reported to form by adding non-interacting molecules such as non-adsorbing polymers.[36] The formation of a polymer-depleted region between two proximal virus particles in the presence of non-interacting polymers induces an osmotic pressure, leading to an attractive interaction between the particles. The spacing of those particles depends on the size and concentration of the non-interacting molecules.[36c] For instance, increasing the concentration of polyethylene glycol (PEG), R_g ~ 4 nm, in the presence of rod-like fd viruses, with a length of 880 nm and diameter of 7 nm, led to their aggregation into hexagonally arranged platelets of several microns in diameter to fibre-like structures with a diameter of one micron and several microns long.[36d] Applications in bio-sensing, such as antibiotic detection after modification of the phages, could be achieved with PEG as a biocompatible molecule that induces anisotropic virus arrangement.[37] These structures can be visualised, for instance, using polarised microscopy and manipulated with optical tweezers, as demonstrated for anisotropic lipid particles in our previous work.[38] The combination of shear-induced alignment of rod-like M13 viruses in polyvinylpyrrolidone as a viscosity modifier led to the formation of fibrous structures similar to those of spider silk.[39] This is an exciting approach

to forming new protein-based fibrous biomaterials for nanofiber fabrication in regenerative tissue medicine or water purification.

3.3 *Colloidal Transformations in the Lipid Envelope of Enveloped Viruses*

Non-enveloped viruses are primarily resistant to alcohol-based disinfectants and surfactants (*e.g.* in soaps).[40] On the contrary, enveloped viruses are susceptible to these compounds.[41] In a recent study in our team, the interaction between ethanol and an enveloped virus pathogen surrogate, the bacteriophage Phi6, was analysed using a combination of SAXS, cryogenic transmission electron microscopy, cryogenic X-ray photon spectroscopy, fluorescence spectroscopy, and biological evaluation studies.[5] The study demonstrated that ethanol mainly acts on the lipid envelope rather than denaturating virus proteins. The virus structure was found intact in the presence of up to 20% ethanol in water. Above 20% ethanol, antiviral activity was observed. SAXS demonstrated that ethanol acts as a co-surfactant, modifying the around 7.5 nm thick lipid envelope structure, which contains the proteins for host–cell recognition. Sufficient ethanol concentrations eventually separated the envelope from the protein cage, resulting in virus inactivation. This fundamental understanding of the antiviral mechanism may allow the design of optimised wide-spectrum antiviral compounds by improving their ability to separate the envelope from the nucleocapsid.

Other amphiphilic molecules have shown to be effective in inactivating enveloped viruses.[42] Surfactants such as sodium oleate, sodium dodecyl sulfate, or Triton X-100 have been shown to disrupt the envelope upon changing the packing parameter of the lipid bilayer. Cationic and amphiphilic antimicrobial peptides such as defensins, histatins, and cathelicidin are also efficient in interacting with the envelope and inactivating enveloped viral pathogens.[43] Thus, the mechanism found for ethanol is likely similar to that of such antiviral molecules.

4. Outlook

The interactions between materials and viruses dictate whether they can be used as antiviral and virus-capture material or virus-based biocomposites. Scattering techniques are precious for gaining fundamental insights into the virus, material structure, and dynamics. Their link with the virus' biological activity can then guide the rational design of advanced virus-based materials. For instance, antiviral polymers need to impair viral bioactivity and may do so by structurally modifying the viral particle or by sterically preventing cell attachment by covering host recognition sites.[44] Alternatively, the inactivation of enveloped viruses can be achieved with compounds such as surfactants or co-surfactants that compromise the function of the lipid envelope.[45]

For virus-based therapy applications, such as phage therapy, various materials that do not change the protein-cage morphology can be used to protect the bacteriophages from harsh environmental conditions allowing them to be antibacterial for a more extensive range of applications.[46] The applications of such materials have been recently reviewed and include bone implant coating, treatment of lung infections, gastrointestinal infections, wound infections, and catheter-related conditions.[7] Each of these applications requires the interaction of the virus with some carrier material, such as the implant surface, the polymeric fibre of wound dressings, or a protective layer against digestive enzymes.

For virus-based biocomposites, the viruses can be rationally designed *via* genetic engineering or *via* a virus (phage) library and selection process to present desired functionalities and self-assembly behaviour.[47] An example of this use is as a scaffold for silica sol.[48] Information about the ordering of the virus in the matrix helps to improve the display of specific functionalities on a surface, such as RGD peptide, for improved cell growth.[49] Further, virus-like particles were used as emulsifiers to prepare protein nanocage-stabilized Pickering emulsions.[50] The protein nanocage cavity could be loaded with antioxidants to act as functional stabilisers for lipids, increasing the shelf life of emulsions. These systems have significant potential as biomimetic materials for health applications and chemical or biotechnological processes. The fundamental understanding of virus self-assembly and stabilisation can unlock key questions in colloid chemistry.

Acknowledgements

The Swiss National Science Foundation supported the work through the NCCR Bioinspired Materials and project no. 186251.

Received: September 5, 2022

[1] J. Rong, Z. Niu, L. A. Lee, Q. Wang, *Curr. Opin. Coll. Interf. Sci.* **2011**, *16*, 441, https://doi.org/10.1016/j.cocis.2011.09.001.
[2] P. Ge, Z. H. Zhou, *Proc. Natl Acad. Sci. USA* **2011**, *108*, 9637, https://doi.org/10.1073/pnas.1018104108.
[3] a) K. Valegard, L. Liljas, 'The Refined Structure of Bacteriophage MS2 at 2.8 Angstroms Resolution', **1995**, https://www.rcsb.org/structure/2MS2; b) R. Golmohammadi, K. Valegård, K. Fridborg, L. Liljas, *J. Mol. Biol.* **1993**, *234*, 620, https://doi.org/10.1006/jmbi.1993.1616.
[4] S. Watts, T. R. Julian, K. Maniura-Weber, T. Graule, S. Salentinig, *ACS Nano* **2020**, *14*, 1879, https://doi.org/10.1021/acsnano.9b08112.
[5] S. Watts, M. Ramstedt, S. Salentinig, *J. Phys. Chem. Lett.* **2021**, *12*, 9557, https://doi.org/10.1021/acs.jpclett.1c02327.
[6] K. E. Gibson, *Curr. Opin. Virol.* **2014**, *4*, 50, https://doi.org/10.1016/j.coviro.2013.12.005.
[7] P. P. Kalelkar, M. Riddick, A. J. García, *Nat. Rev. Mater.* **2022**, *7*, 39, https://doi.org/10.1038/s41578-021-00362-4.
[8] a) W. H. O, 'Situation Report Ebola Virus Disease 10 June 2016', **2016**; b) S. Sullivan, *Lancet* **2018**, *391*, 1242, https://doi.org/10.1016/s0140-6736(17)33292-0; c) W. H. O., 'Coronavirus disease (COVID-19) Weekly Epidemiological Update and Weekly Operational Update', https://www.who.int/emergencies/diseases/novel-coronavirus-2019/situation-reports, accessed 28-oct-2020.
[9] Y. Fan, Y. Wang, *Curr. Opin. Coll. Interf. Sci.* **2019**, *42*, 1, https://doi.org/10.1016/j.cocis.2019.02.011.
[10] C. M. Jeffries, J. Ilavsky, A. Martel, S. Hinrichs, A. Meyer, J. S. Pedersen, A. V. Sokolova, D. I. Svergun, *Nat. Rev. Meth. Primers* **2021**, *1*, 70, https://doi.org/10.1038/s43586-021-00064-9.
[11] A. Ghazal, M. Gontsarik, J. P. Kutter, J. P. Lafleur, D. Ahmadvand, A. Labrador, S. Salentinig, A. Yaghmur, *J. Phys. Chem. Lett.* **2017**, *8*, 73, https://doi.org/10.1021/acs.jpclett.6b02468.
[12] O. Glatter, *J. Appl. Crystallogr.* **1977**, *10*, 415, https://doi.org/10.1107/S0021889877013879.
[13] J. Brunner-Popela, O. Glatter, *J. Appl. Crystallogr.* **1997**, *30*, 431, https://doi.org/10.1107/S0021889896015749.
[14] O. Glatter, *J. Appl. Crystallogr.* **1980**, *13*, 577, https://doi.org/10.1107/S0021889880012794.
[15] O. Glatter, *J. Appl. Crystallogr.* **1981**, *14*, 101, https://doi.org/10.1107/S002188988100887X.
[16] J. S. Pedersen, *Adv. Coll. Interf. Sci.* **1997**, *70*, 171, https://doi.org/10.1016/S0001-8686(97)00312-6.
[17] J. A. Bouwstra, G. S. Gooris, W. Bras, H. Talsma, *Chem. Phys. Lipids* **1993**, *64*, 83, https://doi.org/10.1016/0009-3084(93)90059-c.
[18] O. Glatter, in 'Scattering Methods and their Application in Colloid and Interface Science', **2018**, p. 19, https://doi.org/10.1016/b978-0-12-813580-8.00002-x.
[19] O. Glatter, in 'Scattering Methods and their Application in Colloid and Interface Science', **2018**, p. 33, https://doi.org/10.1016/b978-0-12-813580-8.00003-1.
[20] a) S. Salentinig, S. Phan, T. A. Darwish, N. Kirby, B. J. Boyd, E. P. Gilbert, *Langmuir* **2014**, *30*, 7296, https://doi.org/10.1021/la500835e; b) S. Phan, S. Salentinig, E. Gilbert, T. A. Darwish, A. Hawley, R. Nixon-Luke, G. Bryant, B. J. Boyd, *J. Coll. Interf. Sci.* **2015**, *449*, 160, https://doi.org/10.1016/j.jcis.2014.11.026; c) S. Salentinig, N. R. Yepuri, A. Hawley, B. J. Boyd, E. Gilbert, T. A. Darwish, *Chem. Phys. Lipids* **2015**, *190*, 43, https://doi.org/10.1016/j.chemphyslip.2015.06.007.
[21] O. Glatter, in 'Scattering Methods and their Application in Colloid and Interface Science', Ed. O. Glatter, Elsevier, **2018**, p. 223, https://doi.org/10.1016/B978-0-12-813580-8.00011-0.
[22] R. V. M. Freire, E. Haenni, L. Hong, M. Gontsarik, S. Salentinig, *Adv. Mater. Interf.* **2022**, *9*, 2200446, https://doi.org/10.1002/admi.202200446.

[23] D. Lehner, H. Lindner, O. Glatter, *Langmuir* **2000**, *16*, 1689, https://doi.org/10.1021/la9910273.
[24] a) F. Scheffold, R. Cerbino, *Curr. Opin. Coll. Interf. Sci.* **2007**, *12*, 50, https://doi.org/10.1016/j.cocis.2007.03.005; b) P. N. Pusey, W. Van Megen, *Physica A: Statist. Mech. Appl*. **1989**, *157*, 705, https://doi.org/10.1016/0378-4371(89)90063-0.
[25] a) A. Armanious, M. Aeppli, R. Jacak, D. Refardt, T. Sigstam, T. Kohn, M. Sander, *Environ. Sci. Technol*. **2016**, *50*, 732, https://doi.org/10.1021/acs.est.5b04644; b) B. Michen, T. Graule, *J. Appl. Microbiol*. **2010**, *109*, 388, https://doi.org/10.1111/j.1365-2672.2010.04663.x.
[26] J. Heffron, B. K. Mayer, *Appl. Environ. Microbiol.* **2021**, 87, https://doi.org/10.1128/aem.02319-20.
[27] C. P. Gerba, W. Q. Betancourt, *Environ. Sci. Technol*. **2017**, *51*, 7318, https://doi.org/10.1021/acs.est.6b05835.
[28] O. P. Sahu, P. K. Chaudhari, *J. Appl. Sci. Environ. Manag*e. **2013**, *17*, 241, https://doi.org/10.4314/jasem.v17i2.8.
[29] J. N. Israelachvili, in 'Intermolecular and Surface Forces (Third Edition)', Ed. J. N. Israelachvili, Academic Press, San Diego, **2011**, p. 291, https://doi.org/10.1016/B978-0-12-375182-9.10014-4.
[30] S. Watts, K. Maniura-Weber, G. Siqueira, S. Salentinig, *Small* **2021**, *17*, 2100307, https://doi.org/10.1002/smll.202100307.
[31] N. E. Brunk, M. Uchida, B. Lee, M. Fukuto, L. Yang, T. Douglas, V. Jadhao, *ACS Appl. Bio Mater*. **2019**, *2*, 2192, https://doi.org/10.1021/acsabm.9b00166.
[32] a) A. Matilainen, M. Vepsalainen, M. Sillanpaa, *Adv. Colloid Interface Sci*. **2010**, *159*, 189, https://doi.org/10.1016/j.cis.2010.06.007; b) H. K. Shon, S. Vigneswaran, S. A. Snyder, *Crit. Rev. Env. Sci. Tec*. **2006**, *36*, 327, https://doi.org/10.1080/10643380600580011; c) T. Matsushita, N. Shirasaki, Y. Matsui, K. Ohno, *Chemosphere* **2011**, *85*, 571, https://doi.org/10.1016/j.chemosphere.2011.06.083; d) N. Shirasaki, T. Matsushita, Y. Matsui, T. Marubayashi, *Chem. Eng. J.* **2016**, *284*, 786, https://doi.org/10.1016/j.cej.2015.09.045; e) N. Shirasaki, T. Matsushita, Y. Matsui, T. Marubayashi, K. Murai, *Sci. Total Environ*. **2016**, *563-564*, 29, https://doi.org/10.1016/j.scitotenv.2016.04.090.
[33] M. Uchida, K. McCoy, M. Fukuto, L. Yang, H. Yoshimura, H. M. Miettinen, B. LaFrance, D. P. Patterson, B. Schwarz, J. A. Karty, P. E. Prevelige, B. Lee, T. Douglas, *ACS Nano* **2018**, *12*, 942, https://doi.org/10.1021/acsnano.7b06049.
[34] a) J. Mikkilä, H. Rosilo, S. Nummelin, J. Seitsonen, J. Ruokolainen, M. A. Kostiainen, *ACS Macro Lett*. **2013**, *2*, 720, https://doi.org/10.1021/mz400307h; b) A. Korpi, C. Ma, K. Liu, Nonappa, A. Herrmann, O. Ikkala, M. A. Kostiainen, *ACS Macro Lett*. **2018**, *7*, 318, https://doi.org/10.1021/acsmacrolett.8b00023.
[35] A. K. Tarafder, A. von Kügelgen, A. J. Mellul, U. Schulze, D. G. A. L. Aarts, T. A. M. Bharat, *Proc. Natl Acad. Sci. USA* **2020**, *117*, 4724, https://doi.org/10.1073/pnas.1917726117.
[36] a) Y. Yang, E. Barry, Z. Dogic, M. F. Hagan, *Soft Matter* **2012**, *8*, 707, https://doi.org/10.1039/C1SM06201H; b) T. Li, X. Zan, Y. Sun, X. Zuo, X. Li, A. Senesi, R. E. Winans, Q. Wang, B. Lee, *Langmuir* **2013**, *29*, 12777, https://doi.org/10.1021/la402933q; c) T. Gibaud, *J. Phys.: Cond. Matt*. **2017**, *29*, 493003, https://doi.org/10.1088/1361-648x/aa97f9; d) B. Sung, H. H. Wensink, E. Grelet, *Soft Matter* **2019**, *15*, 9520, https://doi.org/10.1039/C9SM01207A.
[37] J.-S. Moon, M. Park, W.-G. Kim, C. Kim, J. Hwang, D. Seol, C.-S. Kim, J.-R. Sohn, H. Chung, J.-W. Oh, *Sensors and Actuators B: Chem*. **2017**, *240*, 757, https://doi.org/10.1016/j.snb.2016.09.050.
[38] M. Manca, C. Zhang, F. Scheffold, S. Salentinig, *J. Coll. Interf. Sci*. **2022**, *627*, 610, https://doi.org/10.1016/j.jcis.2022.07.028.
[39] R. Sugimoto, J. H. Lee, J.-H. Lee, H.-E. Jin, S. Y. Yoo, S.-W. Lee, *RSC Adv*. **2019**, *9*, 39111, https://doi.org/10.1039/C9RA07510K.
[40] a) G. Kampf, *J. Hosp. Infect*. **2018**, *98*, 331, https://doi.org/10.1016/j.jhin.2017.08.025; b) S. Sato, N. Matsumoto, K. Hisaie, S. Uematsu, *Sci. Rep*. **2020**, *10*, 15878, https://doi.org/10.1038/s41598-020-72609-z.
[41] a) J. M. Boyce, *Infect. Control Hosp. Epidemiol*. **2018**, *39*, 323, https://doi.org/10.1017/ice.2017.301; b) W. H. Organisation, 'WHO Guidelines on Hand Hygiene in Health Care: a Summary', https://www.who.int/gpsc/5may/tools/who_guidelines-handhygiene_summary.pdf; c) Q. Lin, J. Y. C. Lim, K. Xue, P. Y. M. Yew, C. Owh, P. L. Chee, X. J. Loh, *View* **2020**, *1*, https://doi.org/10.1002/viw2.16.
[42] M. Simon, M. Veit, K. Osterrieder, M. Gradzielski, *Curr. Opin. Coll. Interf. Sci.* **2021**, *55*, 101479, https://doi.org/10.1016/j.cocis.2021.101479.
[43] a) K. De Smet, R. Contreras, *Biotechnol. Lett*. **2005**, *27*, 1337, https://doi.org/10.1007/s10529-005-0936-5; b) E. V. Karamov, V. F. Larichev, G. V. Kornilaeva, I. T. Fedyakina, A. S. Turgiev, A. V. Shibaev, V. S. Molchanov, O. E. Philippova, A. R. Khokhlov, *Int. J. Mol. Sci*. **2022**, *23*, https://doi.org/10.3390/ijms23126645.
[44] R. H. Bianculli, J. D. Mase, M. D. Schulz, *Macromolecules* **2020**, *53*, 9158, https://doi.org/10.1021/acs.macromol.0c01273.
[45] a) S. Ghosh, R. Mukherjee, D. Basak, J. Haldar, *ACS Appl. Mater. Interf*. **2020**, *12*, 27853, https://doi.org/10.1021/acsami.9b22610; b) J. Haldar, D. An, L. Álvarez de Cienfuegos, J. Chen, A. M. Klibanov, *Proc. Natl Acad. Sci. USA* **2006**, *103*, 17667, https://doi.org/10.1073/pnas.0608803103.
[46] I. Bajrovic, M. D. Le, M. M. Davis, M. A. Croyle, *J. Control. Rel.* **2022**, *341*, 118, https://doi.org/10.1016/j.jconrel.2021.11.012.
[47] B. Cao, M. Yang, C. Mao, *Acc. Chem. Res*. **2016**, *49*, 1111, https://doi.org/10.1021/acs.accounts.5b00557.
[48] a) M. J. McNulty, N. Hamada, J. Delzio, L. McKee, S. Nandi, M. L. Longo, K. A. McDonald, *J. Nanobiotechnol*. **2022**, *20*, 105, https://doi.org/10.1186/s12951-022-01303-1; b) G. R. Meseck, A. S. Terpstra, M. J. MacLachlan, *Curr. Opin. Coll. Interf. Sci*. **2017**, *29*, 9, https://doi.org/10.1016/j.cocis.2017.01.003.
[49] C. R. Behrens, J. M. Hooker, A. C. Obermeyer, D. W. Romanini, E. M. Katz, M. B. Francis, *J. Am. Chem. Soc.* **2011**, *133*, 16398, https://doi.org/10.1021/ja2033298.
[50] S. Lim, S. Salentinig, *Curr. Opin. Coll. Interf. Sci.* **2021**, *56*, 101485, https://doi.org/10.1016/j.cocis.2021.101485.

License and Terms

The definitive version of this article is the electronic one that can be found at https://doi.org/10.2533/chimia.2022.846